Version of Record: https://www.sciencedirect.com/science/article/pii/S0144860919301177
Manuscript_816773b07e1b3dabc7166bd635fa9648

Numerical modeling of submerged mussel longlines with protective sleeves

Alexander Knysh[a], Igor Tsukrov[a,*], Michael Chambers[a], M. Robinson Swift[a],
Corey Sullivan[a], Andrew Drach[b]

[a] The University of New Hampshire, Durham, NH 03861, USA

[b] The University of Texas at Austin, Austin, TX 78712, USA

* igor.tsukrov@unh.edu

Abstract

Farmers growing mussels in offshore environments have turned to submerged longline farming as a relatively safe, reliable and profitable way to produce mussels in the exposed ocean environment. However, variations in the environmental conditions (strong currents and storms) and potential presence of predator species (e.g. eider ducks) require robust engineering approaches to design longline mussel farms and their components.

This paper describes application of a mechanistic fluid-structure interaction modeling software *Hydro-FE* to predict the dynamic response of several mooring/longline/dropper configurations subjected to typical and extreme environmental conditions of a North Atlantic mussel farming site. *Hydro-FE* is a software tool that expands and modernizes the approach previously implemented in the finite element program *Aqua-FE* developed at the University of New Hampshire to analyze flexible structures in marine environment. The numerical model takes into account smooth variation of the hydrodynamic forces around the free surface (continuous partial submergence), Reynolds number dependence of drag coefficients of mooring lines and includes contributions of predator-protection sleeves to the overall mechanical response of mussel droppers. The simulations provide estimates of anchor forces, mooring line tensions, and time-series data on the motion of the droppers. This information can be used in the design of mussel longlines to prevent anchor failure, rope breakage, line entanglement and mussel fall-off.

Keywords: mussel longline; finite element analysis; fluid-structure interaction; equivalent mussel dropper.

1. Introduction

The aquaculture industry has been continuously expanding to more and more exposed locations worldwide. In particular, mussel farming is becoming popular for nearshore and offshore sites in the United States, Canada and New Zealand. Despite the numerous environmental, economic and jurisdictional difficulties, submerged mussel longline farming turned out to be safe, reliable, profitable and sometimes the only possible way to produce mussels in large quantities (Langan, 2013). Moreover, the submerged longline design (schematically illustrated in Fig. 1) is considered to be superior in terms of expanding to the open ocean environment (Danioux et al., 2000; Buck, 2007; Cheney et al., 2010; Buck and Langan, 2017).

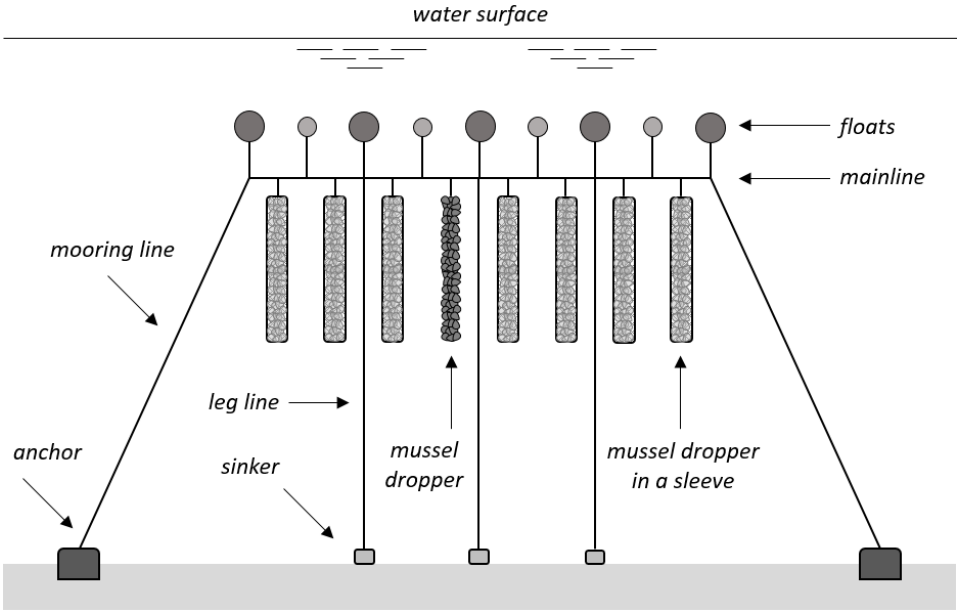

Figure 1. Profile view of an example of a fully-submerged mussel longline with protective sleeves surrounding mussel droppers.

Mussel longlines have been investigated through field observations, scaled physical testing and numerical modeling. There are several valuable observational studies that describe multiday monitoring of the hydrodynamics, loading and motion of mussel longlines in the exposed environment (Stevens et al., 2007; Lin et al., 2016; Gagnon and Bergeron, 2017). Scaled physical experiments in a tank are also important to understand the fluid drag behavior of mussel crop lines as well as implications of such effects as mussel bio-pumping (Plew et al., 2009; Landmann et al., 2019). Dynamic models of mussel

longlines represented by an assemblage of lumped masses connected by springs have been successfully utilized in Raman-Nair and Colbourne, 2003; Raman-Nair et al., 2008. Note that the hydrodynamic behavior and structural performance of mussel longlines with protective sleeves are similar to other longline culture systems, such as oysters or scallops, with lantern nets. The examples of numerical and physical modeling of such systems are provided in López et al., 2017; Zhao et al., 2019, with a comprehensive literature review on the topic found in Zhao et al., 2019.

In this paper, finite element analysis in applied to evaluate a set of simple one-line designs of submerged mussel growing installation. There are several finite element modeling software packages available to analyze flexible aquaculture structures in marine environment. Commercially available programs, *OrcaFlex* (https://www.orcina.com/) and *ProteusDS* (https://dsa-ltd.ca/proteusds/overview/), provide robust user interface and strong validation background for various ocean engineering applications. The finite element software package *AquaSim* was developed specifically for net modeling and aquaculture applications (Berstad et al., 2012; Berstad and Heimstad, 2019). The fish cage aquaculture farm modeling programs developed at Dalian University of Technology (Li et al., 2006; Zhao et al., 2007, 2015), SINTEF Fisheries and Aquaculture (Reite et al., 2014; Tsarau and Kristiansen, 2019) and Pukyong National University (Lee et al., 2008, 2015) are based on a lumped-mass representation and a direct dynamic modeling approach.

The software package used in the present paper, *Hydro-FE*, is based on the well-validated *Aqua-FE* software developed at the University of New Hampshire (Gosz et al., 1996; Tsukrov et al., 2000; Fredriksson et al., 2003). The purpose of this study is to evaluate several simple longline and dropper sleeve designs, and to estimate the influence of the design modifications on the overall structural response. Environmental conditions include current and waves which are implemented using Airy wave theory (Dean and Dalrymple, 1991). Hydrodynamic forcing on mooring lines is calculated with Reynolds number dependent drag coefficients (Choo and Casarella, 1971; DeCew et al., 2010). The equivalent dropper model is developed and utilized to improve computational performance. A set of parametric studies is performed to evaluate sensitivity of the results to the mussel droppers' drug coefficients and bending stiffness.

The rest of the paper is organized as follows. Section 2 describes the designs of the considered mussel farms and the properties of the droppers as defined by their mussel protection sleeves. The concept of an equivalent mussel dropper used in the numerical modeling is introduced in Section 3. The section also includes description of the finite element models of all four considered designs. Section 4 provides the environmental conditions of the mussel farming site and the available data on the dropper

drag coefficients. The results of numerical simulations including the parametric studies for drag coefficient and bending stiffness contributions are presented in Section 5.

2. Mussel farm design

2.1 Mussel longlines

Most modern mussel longline farms consist of rows of vertical droppers hanging from mainlines which are supported by a set of floats and fixed by mooring lines (Drapeau et al., 2006; Buck, 2007; Karayücel et al., 2015). Sometimes, vertical legs with sinkers and floats are also added for dynamic stability (Gagnon and Bergeron, 2017). The dropper itself consists of a polyester core rope with an outer layer of fibrous material that is conducive to mussel spat collection and settlement. The mussels attach to the fibrous material as larvae and then attach to the inner core rope as they grow. The mussels are sometimes enclosed into a meshed sleeve to protect them from various predators, such as diving eider ducks. These sleeves can affect the mussel growth and the resulting mechanical properties of the droppers.

In this study, the performance of a fully submerged longline with 80 droppers uniformly distributed along the mainline (as shown in Fig. 2) was investigated by direct numerical modeling. This particular configuration was utilized by Peter Flanigan and Vincent Prien from Isles of Shoals Mariculture, off the coast of Rye, New Hampshire, USA. The mainline was maintained in an approximately horizontal position by appropriately distributing $325\ N$ floats each (the number of floats varied from 21 to 53 depending on the droppers' linear density and mooring design). The longline was deployed in $33\ m$ depth, $11\ m$ below water surface. The length of the mainline was $73\ m$; the droppers were $3\ m$ long; the distance between the anchors was $152\ m$. More information on geometric and mechanical properties of the components is provided in Section 3.3.

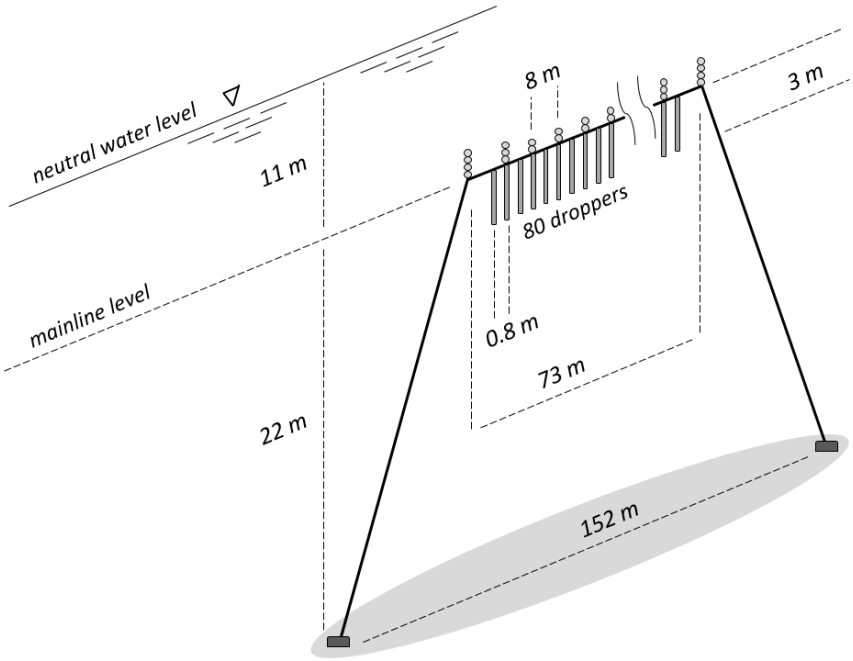

Figure 2. Isometric view of the mussel longline with two mooring lines.

Preliminary simulations showed that the design illustrated in Fig. 2 experienced excessive motion in extreme storm conditions as described in Section 5. In an attempt to better control the system dynamics, three modification of the original 2-point mooring design were considered, as presented in Table 1. The first modification of the initial structure, "4-point mooring", has 2 anchors at each end (4 in all). Each anchor pair is spread out on the bottom along a line perpendicular to the mainline. The anchors are located $24\ m$ apart at the same distance of $152\ m$ from the opposite pair of anchors. The mooring lines converge to the end of the mainline forming an inverted "V". The second modification, "4-point mooring with weights" or "4-point mooring [W]", includes an extra $38\ kg$ ballast weight attached to the lower end of each dropper as well as an additional row of floats to compensate for it. Finally, the third modification, "4-point mooring with vertical legs" or "4-point mooring [VL]", is constrained with 3 additional leg lines: one is at the middle and two others are $20\ m$ away from the corresponding ends of the mainline. A more detailed description of these modifications, including mechanical and geometrical properties of the components, is provided in Section 3.3.

Table 1. Variations of the longline design considered in this paper.

Design	**Mooring lines**	**Vertical Leg lines**	**Additional weight**
2-point mooring	2	0	No
4-point mooring	4	0	No
4-point mooring [W]	4	0	Yes

4-point mooring [VL]	4	3	No

2.2 Properties of mussel droppers with three types of protective sleeves

A research project initiated by National Oceanic and Atmospheric Administration and local mussel farming industry in 2017 aims to grow the offshore mussel industry in the Gulf of Maine by developing longline systems that can survive biological (eider predation) and physical (high wave energy) constrains. Its objectives are to evaluate new protective technologies and strategies that will allow to grow mussels without constriction and prevent diving ducks from preying upon shellfish during their seasonal migrations, and to transfer protective shellfish methods and relevant business planning information to new and existing farmers in New England.

Protective sleeves are not commonly used in the mussel longline farming but can protect shellfish droppers from various predators. Typical sleeves are made of plastic and installed in such a way as to fully cover the mussel droppers. Three types of protective sleeves made of low density polyethylene and manufactured by Industrial Netting, USA (https://www.industrialnetting.com/) have been tested with regards to their performance for mussel growing applications. They included NG 8060 Standard Duty yellow, NG3070 Vexar Work Grade blue and NG2090 Vexar Superduty green sleeves (https://www.industrialnetting.com/parts-protection.html). The sleeves vary in their rigidity and cell size. In the text to follow, mussel droppers with these sleeve types are referred to as *green*, *blue* and *yellow*, respectively. As an example, the structure of the *green* dropper can be seen in Fig. 3c. There are also sleeves manufactured by Intramas Group, Spain that are currently in use but were not tested in this paper (https://www.intermasgroup.com/about-us/our-locations/spain/intermas-nets.html).

Measurements of the mechanical and geometric properties of the mussel droppers in these sleeves were taken on July 3, 2018 at the University of New Hampshire nearshore multi-trophic aquaculture site in the mouth of the Piscataqua River in New Castle, New Hampshire, USA, see Fig. 3a. The *green* dropper was first seeded in March 2017 with a secondary seeding occurring in October 2017, and the *blue* and *yellow* droppers were only seeded in October 2017. The protective meshes were also applied to the droppers at different times. The green and blue meshes were applied in November 2017, and the yellow mesh was applied in February 2018.

Presence of the protective sleeves and the different seeding dates affected the overall diameter, density and bending stiffness of each mussel dropper. The diameter for each dropper type was recorded as the average of three measurements $d_h = \frac{1}{3}\left(d_h^{(1)} + d_h^{(2)} + d_h^{(3)}\right)$. The linear density was calculated from

the weight W of the suspended portion of the dropper l_w in the air $\omega_{air} = \frac{W}{g l_w}$. The bending stiffness was determined using a cantilever beam model by freely suspending a portion of a dropper ($l_b = 0.33\ m$) from a horizontal support, see Fig. 3b. The deflection δ of the free end due to self-weight was measured. Then, using the strength of materials formula for a cantilever beam under a uniformly distributed loading (Bansal, 2010), the dropper's bending stiffness EI was found as

$$EI = \frac{\omega_{air}\, g\, l_w^4}{8\, \delta} \quad , \tag{1}$$

where g is the gravity constant. It was determined that the bending stiffness of the *yellow* dropper was $0.79\ N \cdot m^2$, while the *blue* and *green* ones had negligible bending stiffness. The results of all measurements are summarized in Table 2.

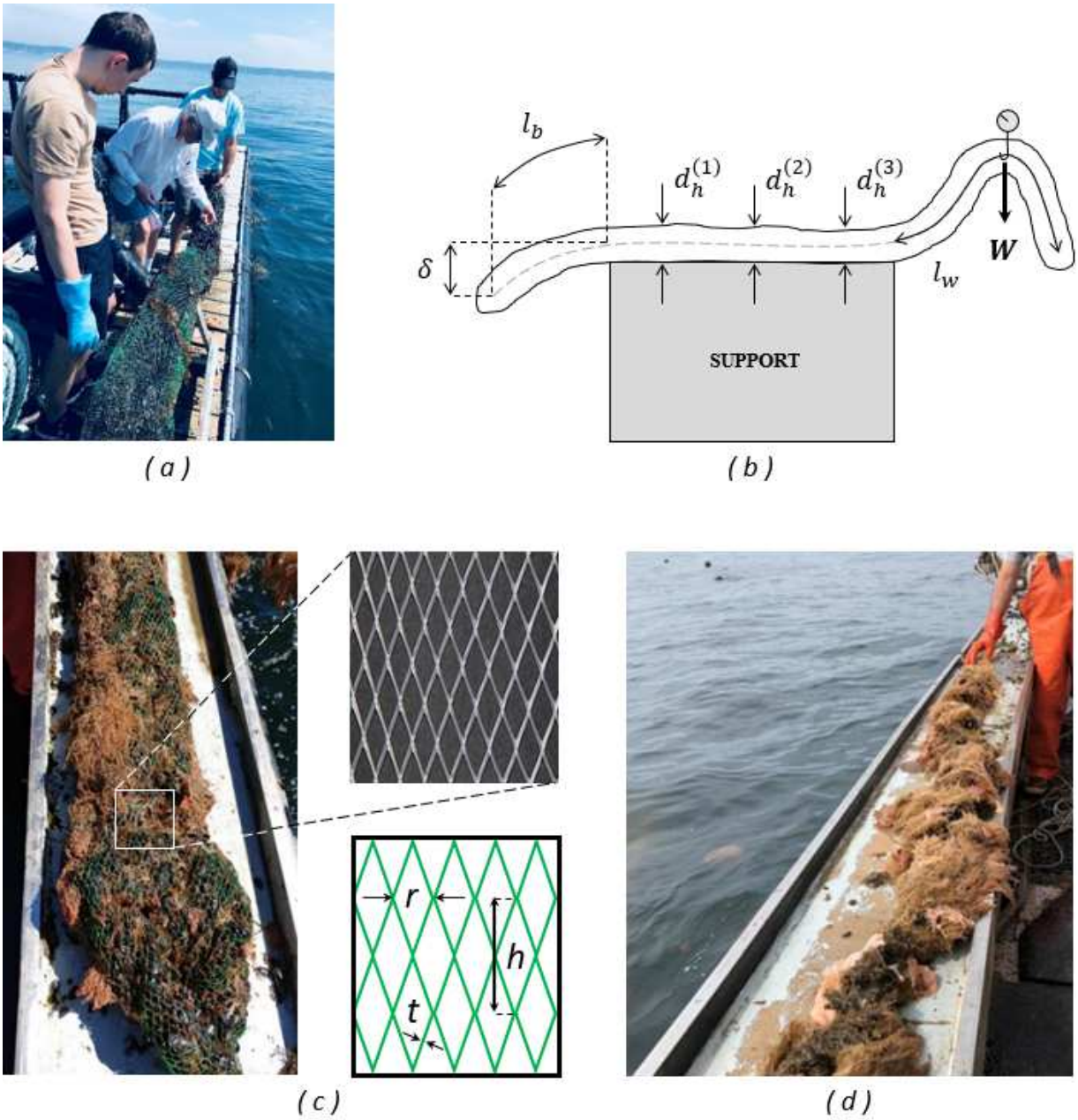

Figure 3. Inspection and measurements of the droppers' density and bending stiffness: *(a)* field measurements on July 3, 2018; *(b)* schematics of the measurements on July 3, 2018; *(c)* farm inspection on May 9, 2019 – mussels in *green* dropper; (d) farm inspection on July 24, 2019 – the control dropper without sleeve void of mussels and overgrown with tubularia.

Table 2. Field measurements and calculated parameters of droppers.

Sleeve type	Twine thickness t [cm]	Mesh cell width r [cm]	Mesh cell height h [cm]	Diameter of dropper d_h [m]	Linear density ω_{air} [kg/m]	Bending stiffness EI [$N \cdot m^2$]
Yellow	0.10	1.54	2.85	0.13	7.53	0.79
Blue	0.11	1.49	2.80	0.13	9.00	*negligible*
Green	0.13	1.42	2.71	0.25	17.71	*negligible*

Measurements conducted on July 3, 2018 correspond to the intermediate state of the mussel growing cycle. Previous studies reported the average values of a dropper diameter varying from $0.12\ m$ to $0.2\ m$ (Plew et al., 2005; Stevens et al., 2007; Cranford et al., 2014; Gagnon and Bergeron, 2017), depending on the environmental conditions, farm design, and mussel species. As mussels grow, the average diameter and weight of the dropper can increase by approximately 5-10% every 40 days of growth (Lauzon-Guay et al., 2006; Gagnon and Bergeron, 2017). Fig. 3c produced during the mussel farm inspection on May 9, 2019 illustrates the state of the *green* dropper when the sleeve is completely filled with mussels. Note that for numerical simulations presented in this paper, the geometrical and mechanical properties measured on July 3, 2018 are used. As the culture grows and the properties change, it has to be reflected in the input data of the model.

During the regular farm inspections, it was observed that the presence of predator-protection sleeves provides surface area for biofouling organisms to attach. However, with the filter feeding mussels near the sleeve, biofouling attachment was minimized as shown in Fig. 3c compared to unprotected control droppers in Fig. 3d. The control dropper without the sleeve was void of mussels and overgrown with tubularia. Much less biofouling was observed on the *green* dropper filled with mussels (Fig. 3c). It appears that the filter feeders inside the net were able to consume the free floating hydroid larvae before they even settle. This situation is different from the lantern nets where large areas of the exposed netting material provide more surface for the tubularia to attach.

3. Concept of an equivalent dropper

The finite element discretization required for numerical modeling of longline farms with a large number of mussel droppers can lead to an excessive number of finite elements, resulting in unreasonable simulation time and costs. To simplify the numerical models without significant loss of accuracy, the

concept of an "equivalent dropper" representing several actual droppers was utilized. This approach mimics the concept of "consistent net elements" described in Tsukrov et al., 2002. The equivalent dropper should have the same weight, buoyancy and hydrodynamic performance as several actual droppers. In this section, the required geometric and physical parameters of an actual mussel dropper are identified, and then an approach to selecting the equivalent dropper values is proposed. Note that since water permeates the dropper, the buoyancy force acting on the dropper of length L it will not be equal to $\pi\rho_w L d_h^2/4$, where ρ_w is the water density and d_h is the diameter obtained from the measurements. To properly account for this effect, two separate diameters are introduced: the "hydrodynamic" diameter d_h, which is obtained from the measurements and used for estimating hydrodynamic forces, and the "structural" diameter d_s, which is calculated to represent the dropper's axial stiffness, mass and buoyancy.

3.1 Modeling of the actual mussel dropper

The simplest possible approach is to consider a dropper as a homogeneous flexible cylinder. In this case, its diameter and density can be determined from direct measurements (Fig. 3). For example, our field measurements of the *yellow* dropper resulted in a linear density in the air of $\omega_{air} = 7.53\ kg/m$ and an outer diameter of $d_h = 0.13\ m$.

However, mussel droppers are porous, so that the outer diameter d_h will not represent the amount of water displaced by the dropper. Thus, it cannot be used to evaluate buoyancy and inertia of the dropper in the water. One additional measurement is needed. If the linear density of the dropper measured in air is ω_{air} and the linear density of the submerged dropper is ω_{subm}, the buoyancy correction coefficient k can be introduced as $\omega_{subm} = k\ \omega_{air}$. Recent studies show that the buoyancy correction coefficient for a dropper with blue mussels is around 0.25 (Dewhurst, 2016). Then, based on Archimedes' principle, the average density of the dropper material is defined by:

$$\rho_d = \frac{\rho_w}{1-k}\ . \tag{2}$$

In this case, the mass of the dropper will be $\rho_d V_{dropper} = \rho_d(\pi\ L\ d_s^2)/4$ which results in the following estimate of the structural diameter:

$$d_s = \sqrt{\frac{4\ \omega_{air}}{\pi\ \rho_d}}\ , \tag{3}$$

where d_s can be used to calculate the overall weight and buoyancy of the dropper, while d_h is used for hydrodynamic forces. The abovementioned distinction is implemented in *Hydro-FE* by introducing a buoyancy adjustment multiplier $k_b = d_s^2/d_h^2$ as a ratio of nominal and actual volumes of the mussels in the dropper.

3.2 Equivalent mussel dropper

Consider one equivalent mussel dropper which represents N actual ones, and has the same average density ρ_d and length L. To keep the total droppers' mass, the linear density of the equivalent dropper should be $\tilde{\omega}_{air} = N\omega_{air}$. Applying (3) to the equivalent dropper, the equivalent structural diameter becomes

$$\tilde{d}_s = \sqrt{\frac{4\,\tilde{\omega}_{air}}{\pi\,\rho_d}} = \sqrt{N}\,d_s \ . \tag{4}$$

The hydrodynamic diameter of an equivalent dropper, $\tilde{d}_h$, is chosen to represent the total drag and inertia forces exerted on N actual droppers. In order to calculate this force, the Morison equation approach (Morison et al., 1950), expanded to the case of a moving cylinder (Goodman and Breslin, 1976) is used. Consider a submerged equivalent dropper of diameter $\tilde{d}_h$ arbitrarily moving in the water (Fig. 4) and subdivided into differential sections dL. There are two vectors associated with each of those sections: the local fluid velocity vector $\boldsymbol{u}$ and the body velocity vector $\boldsymbol{v}$. Both of these vectors can be projected on tangential (parallel to the cylinder axis) and normal (perpendicular to the cylinder axis) directions. Then, the normal projection of the force exerted on a differential section dL is

$$d\widetilde{\boldsymbol{F}}_n = \rho_w \frac{\partial \boldsymbol{u}_n}{\partial t} d\tilde{V} + C_a \rho_w \left(\frac{\partial \boldsymbol{u}_n}{\partial t} - \frac{\partial \boldsymbol{v}_n}{\partial t}\right) d\tilde{V} + \frac{1}{2} C_d \rho_w |\boldsymbol{u}_n - \boldsymbol{v}_n|(\boldsymbol{u}_n - \boldsymbol{v}_n) d\tilde{A} \ , \tag{5}$$

where $\boldsymbol{u}_n$ and $\boldsymbol{v}_n$ are the normal projections of fluid and body velocities associated with section dL, C_a is the added mass coefficient, C_d is the normal drag coefficient, $d\tilde{V}$ and $d\tilde{A}$ are the equivalent differential volume and the normal projected area of section dL. The tangential component of the drag force is taken in the form:

$$d\widetilde{\boldsymbol{F}}_t = \frac{\pi}{2} C_t \rho_w |\boldsymbol{u}_t - \boldsymbol{v}_t|(\boldsymbol{u}_t - \boldsymbol{v}_t) d\tilde{A} \ , \tag{6}$$

where C_t is the tangential drag coefficient, $\boldsymbol{u}_t$ and $\boldsymbol{v}_t$ are the tangential projections of fluid and body velocities associated with section dL. The differential volume and the normal projected area are calculated as

$$d\tilde{V} = \tilde{S} dL = \frac{1}{4}\pi \tilde{d}_h^2 dL \ ,$$

$$d\tilde{A} = \tilde{d}_h dL \ . \tag{7}$$

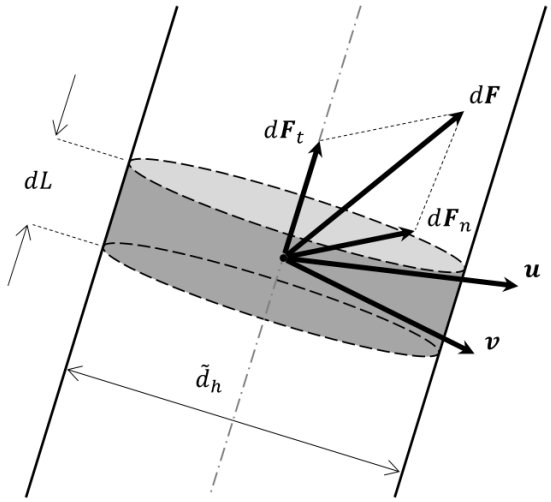

Figure 4. Moving equivalent dropper in a time-dependent water flow; direction t is along the cylinder, plane n is perpendicular to it.

Formulas (5) and (6) show that the normal component of the total hydrodynamic force acting on the equivalent dropper depends on both the equivalent volume and the equivalent projected area, while the tangential component depends on the entire side area $\pi d\tilde{A}$. It is not possible to pick such a value of $\tilde{d}_h$ that $\widetilde{\boldsymbol{F}}_n = N\boldsymbol{F}_n$ and $\widetilde{\boldsymbol{F}}_t = N\boldsymbol{F}_t$ since $d\tilde{V}$ and $d\tilde{A}$ depend on the equivalent diameter quadratically and linearly, respectively. The described contradiction is resolved by determining $\tilde{d}_h$ from the equality of the equivalent and actual droppers' volumes $d\tilde{V} = NdV$, and then introducing the drag adjustment multiplier k_d, that equalizes the equivalent and actual projected areas $k_d d\tilde{A} = NdA$:

$$\tilde{d}_h = \sqrt{N} d_h \ ,$$

$$k_d = \sqrt{N} \ . \qquad (8)$$

The drag adjustment multiplier k_d is implemented as a parameter in *Hydro-FE* software. Note that the buoyancy adjustment multiplier for the equivalent dropper expressed similarly as for the actual dropper $k_b = \tilde{d}_s^2 / \tilde{d}_h^2$.

The bending stiffness of the equivalent dropper is prescribed to have the same horizontal deflection Δ of the lower end as for the actual dropper when fixed at the upper end and subjected to the same horizontal current, see Fig. 5. This deflection is proportional to the distributed loading, exerted on the dropper by the fluid, which is proportional to the projected area of the dropper since the first two terms in right-hand side of (5) are zeroes. With the actual and equivalent areas being related as $d\tilde{A} = \sqrt{N} dA$, we obtain:

$$\widetilde{EI} = \sqrt{N}\, EI \ . \tag{9}$$

The concept of the equivalent dropper approach is validated in Section 5.1.

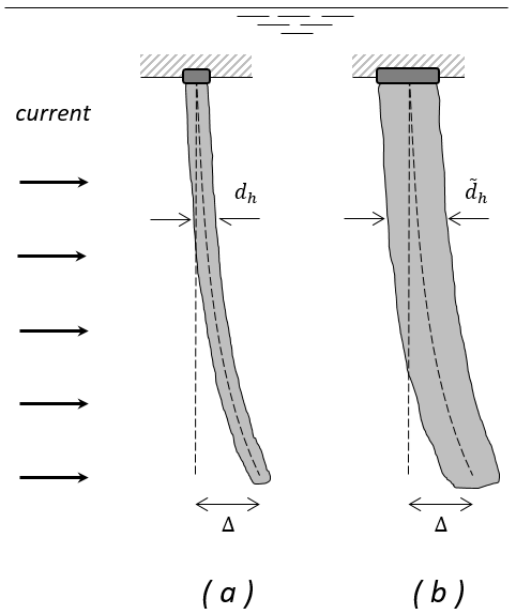

Figure 5. Deflection of *(a)* actual and *(b)* equivalent dropper under a uniform current loading.

3.3 Finite element models of mussel longlines

In this study, the longline system is numerically investigated via finite element simulations. Finite element models were built for all design variations presented in Table 1. However, direct modeling of 80 droppers would make the finite element model computationally inefficient due to a high number of finite elements associated with the droppers. For this reason, every 10 droppers in the longline models are represented by an equivalent one, according to the equivalent dropper concept described in Section 3.2. There are four structural components present in the designs: ropes, equivalent droppers, floats and weights (for the weighted configuration only). The mechanical and geometric properties of these components are provided in Table 3. Note that the bending stiffness of the droppers is found from the experiments described in Section 2 independently from the axial Young's modulus presented in Table 3. The values of the Young's modulus for floats and weights have been selected to be much higher than other structural components as they are stiffer and don't significantly influence the overall dynamic response.

In the considered designs, the number of float elements depends on the dropper type because *yellow*, *blue* and *green* droppers have different mass and, as a result, require specific number of floats to

be properly supported (one float is always represented by one finite element). The designs also differ in the number of elements related to the rope and weight (Table 4).

Schematics of the finite element models are shown in Fig. 6. Going from design *(a)* to design *(b1)* adds 2 additional mooring lines or 40 elements; from *(b1)* to *(b2)* – adds 8 weights, 9 floats and 9 ropes to connect floats or 26 elements; from *(b2)* to *(c)* – adds 3 legs, removes 2 floats and 8 weights or additional 45 elements in total.

Table 3. Mechanical and geometric properties the mussel longline structural components used in the finite element model.

Structural component	**Density** $[\ kg/m^3\ ]$	**Young's modulus** $[\ GPa\ ]$	**Diameter** $[\ m\ ]$	**Element type**
Rope	930	0.69	0.025	2-node, 3-d, truss
Equivalent dropper ***(yellow / blue / green)***	1366	0.1	*0.26 / 0.29 / 0.40*	2-node, 3-d, *beam / truss / truss*
Float	37	1	0.32	2-node, 3-d, truss
Weight	8050	100	0.17	2-node, 3-d, Truss

Table 4. Number of finite elements used for each structural component of the mussel longline designs

Structural component	**2-point mooring**	**4-point mooring**	**4-point mooring [W]**	**4-point mooring [VL]**
Rope	154	194	203	258
Equivalent dropper	80	80	80	80
Float ***(yellow / blue / green)***	*21 / 24 / 44*	*21 / 24 / 44*	*30 / 33 / 53*	*28 / 31 / 51*
Weight	-	-	8	-
Total number of	*255 / 258 / 278*	*295 / 298 / 318*	*321 / 324 / 344*	*366 / 369 / 389*

elements				

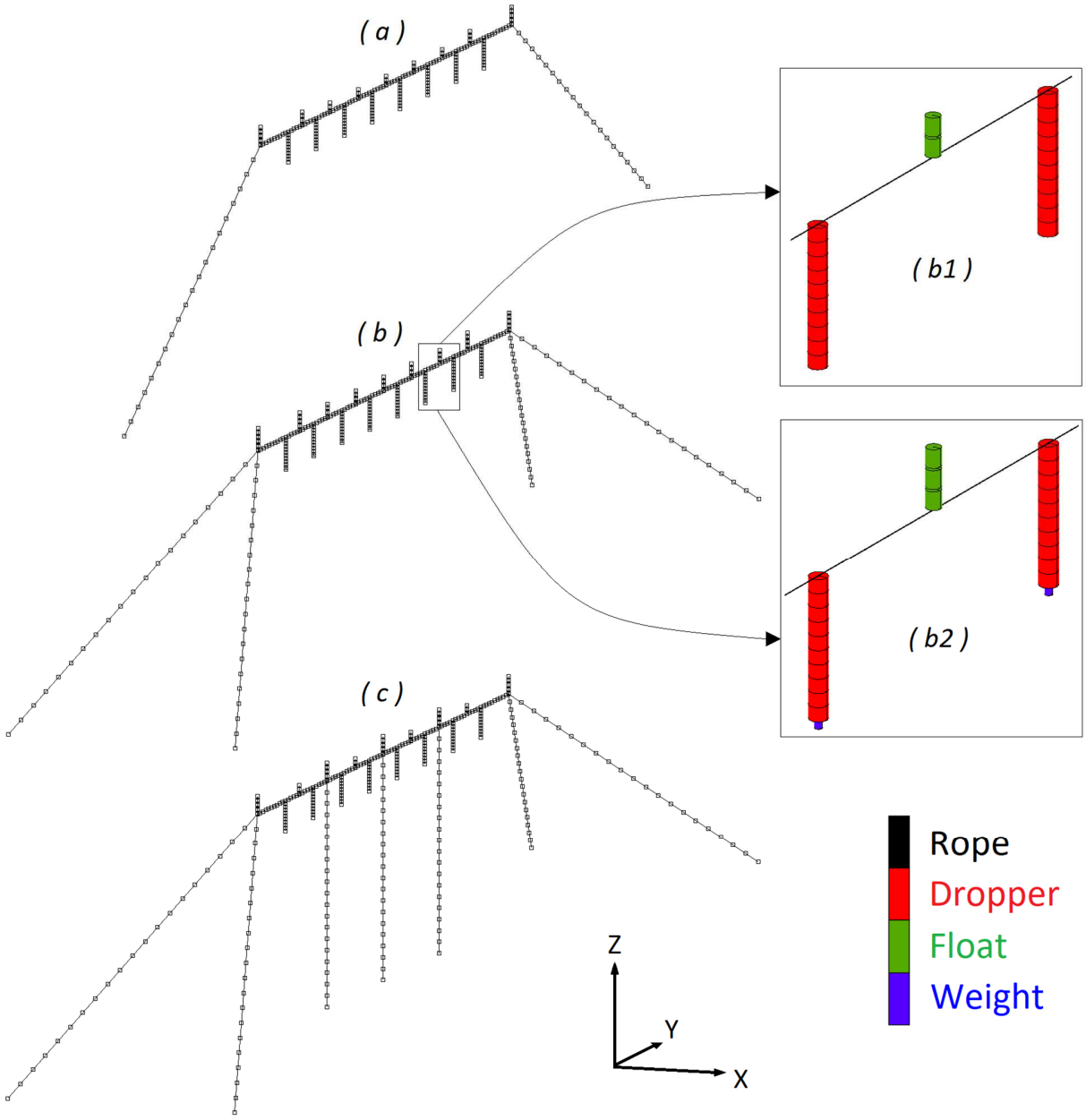

Figure 6. Finite element models of longlines with equivalent droppers: *(a)* 2-point mooring design; *(b, b1)* 4-point mooring design; *(b, b2)* 4-point mooring [W] design; *(c)* 4-point mooring [VL] design.

4. Environmental conditions and drag coefficients

4.1 Environmental conditions

There are two representative North Atlantic mussel farming site weather conditions considered in the study: fair weather and storm. Both of them are characterized by a current velocity and monochromatic wave properties shown in Table 5. Note that the wave length L was found using the dispersion equation of linear wave theory (Dean and Dalrymple, 1991)

$$\sigma^2 = gk\,tanh(kh)\ , \tag{10}$$

where $\sigma = 2\pi/T$ is the wave frequency, $k = 2\pi/L$ is the wave number, T is the wave period, h is the depth of water. The current velocity and wave propagation vectors were assumed to be collinear. In this study, random waves were not considered. The case of monochromatic waves collinear with the current and perpendicular to the longline was the extreme case chosen because the difference in hydrodynamic behavior of different designs is more pronounced for such a loadcase.

Table 5. Current and wave properties of characteristic environmental conditions.

Weather	**Current velocity** [$\boldsymbol{m/s}$]	**Wave height** [$\boldsymbol{m}$]	**Wave period** [$\boldsymbol{s}$]	**Wave length** [$\boldsymbol{m}$]
Fair	0.15	1	4	25
Storm	0.15	5	8.8	114.9

4.2 Drag coefficients

In most of the published numerical studies, mussel droppers are modeled as rigid or flexible cylinders, see, for example (Raman-Nair and Colbourne, 2003; Plew, 2005; Cranford et al., 2014). Hydrodynamic forces on these cylinders are usually described by the Morison equation (5) with the values of normal drag and added mass coefficients taken either from experimental data or based on the assumption of a smooth cylinder (Hoerner, 1965). Sometimes, normal drag coefficients of mussel droppers are assumed to be similar to ultra-rough cylinders with $C_{dn} = 1.7$ (Plew et al., 2005; Stevens et al., 2008).

A more rigorous investigation of the drag was conducted with artificial mussel crop rope and provided an estimate of $C_{dn} = 1.3$ for Reynolds number from 1×10^4 to 7×10^4 (Plew et al., 2009). These values were used, for example, in a submersible mussel raft dynamics research (Dewhurst, 2016).

Recent experiments with live mussel droppers (Landmann et al., 2019) resulted in mean normal drag coefficients of $1.16 - 3.03$ for Reynolds numbers from 2×10^4 to 1.1×10^5. The authors of that publication observed that the drag coefficients increase with decrease of Reynolds number. The results of the abovementioned studies are summarized in Table 6. Note that no significant variations in the added mass and tangential drag coefficients of mussel dropper have been reported. To the best of the authors' knowledge, these properties of a mussel dropper are relatively unexplored and require further investigation.

Table 6. Reported values of normal drag C_{dn} and tangential drag C_{dt} coefficients for a mussel dropper. Added mass coefficient is denoted as C_a.

Source	C_{dn}	C_{dt}	C_a
Raman-Nair and Colbourne, 2003	1.5	-	-
Plew, 2005	1.1	-	1
Raman-Nair et al., 2008	1.2	0.1	-
Stevens et al., 2008	1.7	-	-
Plew et al., 2009	1.3	-	-
Dewhurst, 2016	1.3	-	1
Gagnon and Bergeron, 2017	1.1	0.08	-
Landmann et al., 2019	1.16-3.03	-	0.25-1.25

Our numerical studies show that predictions for mooring line tensions and the overall longline dynamics are not very sensitive to the exact choice of the normal and tangential drag coefficients, if they are taken within a reasonable range of values, see Section 5.2. The results reported in Section 5 correspond to the Reynolds number of 4×10^4 and greater. The values $C_{dn} = 1.3$, $C_{dt} = 0.1$, $C_a = 1$ were adopted unless otherwise specified.

5. Performance of submerged mussel longline in a high energy environment

5.1 Equivalent dropper concept validation

In order to validate the equivalent dropper approach in terms of the dynamic (tension, reaction force) and kinematic (displacement, velocity, acceleration) responses, the numerically predicted behavior of the initial 2-point mooring configuration with 80 actual *yellow* droppers (Fig. 7a) was compared to 8

equivalent ones (Fig. 7b) subjected to the same fair weather condition, so each equivalent dropper represents hydrostatic and hydrodynamic forces acting on 10 equivalent droppers, see Section 3.

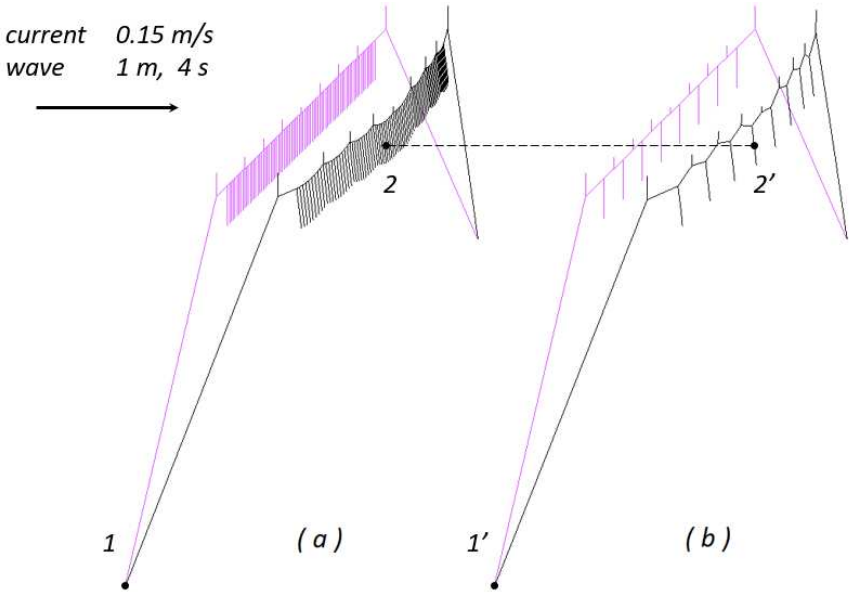

Figure 7. Initial and deformed state of the 2-point longline design under the fair environmental condition with: *(a)* actual *yellow* droppers; *(b)* equivalent *yellow* droppers. The deformed state corresponds to the maximum deflection from the initial position. Points *1* and *1'* are the mooring line attachments. Points *2* and *2'* are at the middle of the 4th dropper.

Table 7 presents maximum mooring line tension T at points *1* and 1', horizontal displacement d_x, absolute value of velocity v and absolute value of acceleration a at points 2 and 2', where locations *1, 1', 2* and *2'* are provided in Fig. 7. Numerical simulations show good agreement between actual and equivalent finite element models (Fig. 8) with less than 5% difference in maximum values (Table 7). The maximum values of T, d_x, v and a have a special interest for ocean engineers since they usually serve as a general criterion for reliability, durability and performance of a longline mussel farm structure (Raman-Nair and Colbourne, 2003; Raman-Nair et al., 2008). For this particular configuration, the equivalent dropper approach provides more than 3.5 times speed-up of numerical calculation when performed with *Intel® Core™ i7-3770, 3.40 GHz* processor on 2 cores.

Table 7. Maximum values of tension, displacement, velocity and acceleration of actual and equivalent longline models.

Dropper type	$T\ [kN]$	$d_x\ [m]$	$v\ [m/s]$	$a\ [m/s^2]$
Actual dropper	2.44	7.22	0.061	0.093
Equivalent	2.48	7.16	0.060	0.097

dropper				
Difference	1.9 %	0.8 %	1.6 %	4.3 %

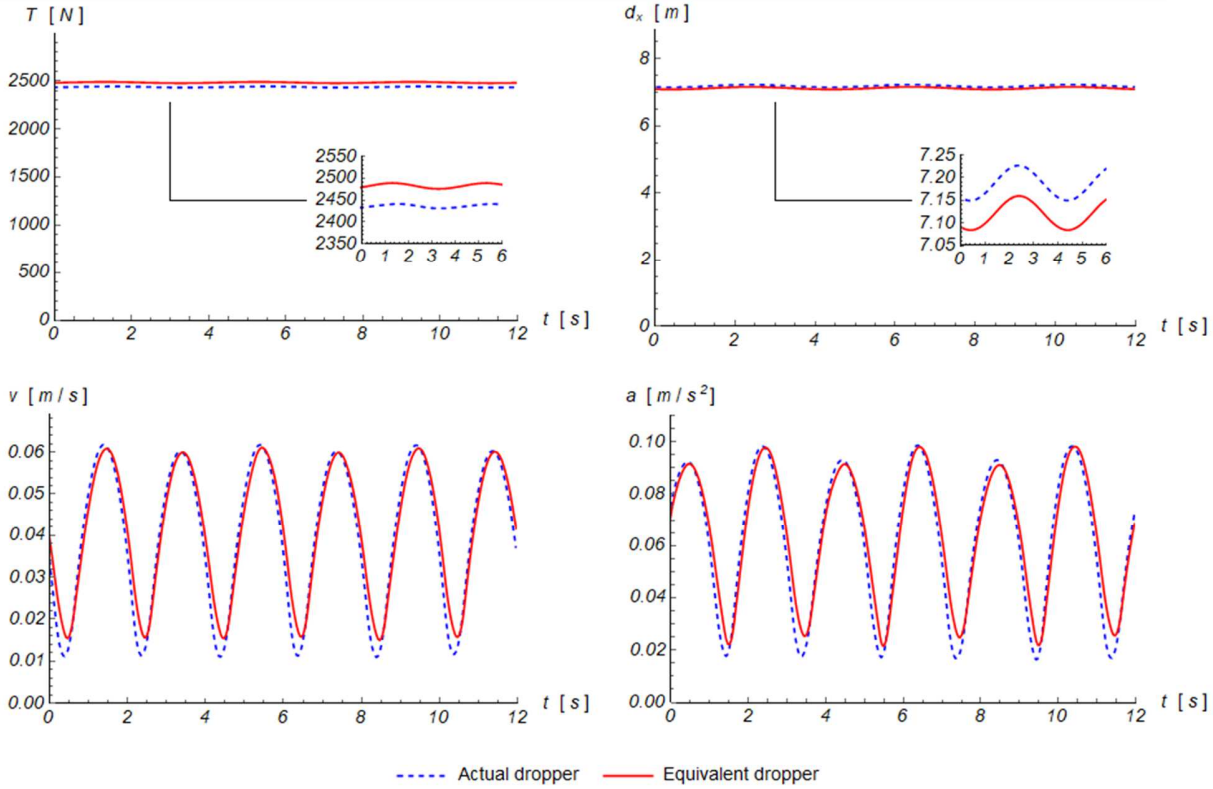

Figure 8. Comparison between actual and equivalent longline model response in fair weather. T is the mooring tension, and displacements d_x, velocities v and acceleration a are provided for the midpoint of the 4th dropper.

5.2 Parametric studies for drag coefficient and bending stiffness contribution.

In this section, the sensitivity of the numerical predictions to the exact choice of the dropper drag coefficient and bending stiffness is investigated. The 4-point mooring design with *yellow* droppers under the storm conditions was selected for the parametric study. Since most of the reported normal drag coefficients are $1.1 \leq C_{dn} \leq 1.7$, there were four models chosen for the study based on the dropper's C_{dn} and the element type: $C_{dn} = 1.1$ with truss elements; $C_{dn} = 1.1$ with beam elements; $C_{dn} = 1.7$ with truss elements; $C_{dn} = 1.7$ with beam elements. These cases were compared with each other and with the benchmark $C_{dn} = 1.3$ with beam element case.

Fig. 9 provides mooring tension at anchor point 1' and kinematic response point 2', where the location of points is shown in Fig. 8b. It can be seen in Table 8 that the maximum deviation from the parameters chosen in the performance study ($C_{dn} = 1.3$ with beam elements) does not exceed 7.6% in

terms of highest tension, 5.5% in displacement, 1.3% in velocity and 1.7% in acceleration. This parametric study shows that the combined effect of perturbing the drag coefficient by ± 30% and switching on and off the effect of bending stiffness in the model are bound by well-defined narrow intervals in all of the considered quantities of interest. For all practical intents and purposes, these bounds are within the expected variations of the experimental measurements, and thus these parameters can be fixed in the midrange value and their variations deemed statistically insignificant to the variations in the predicted results.

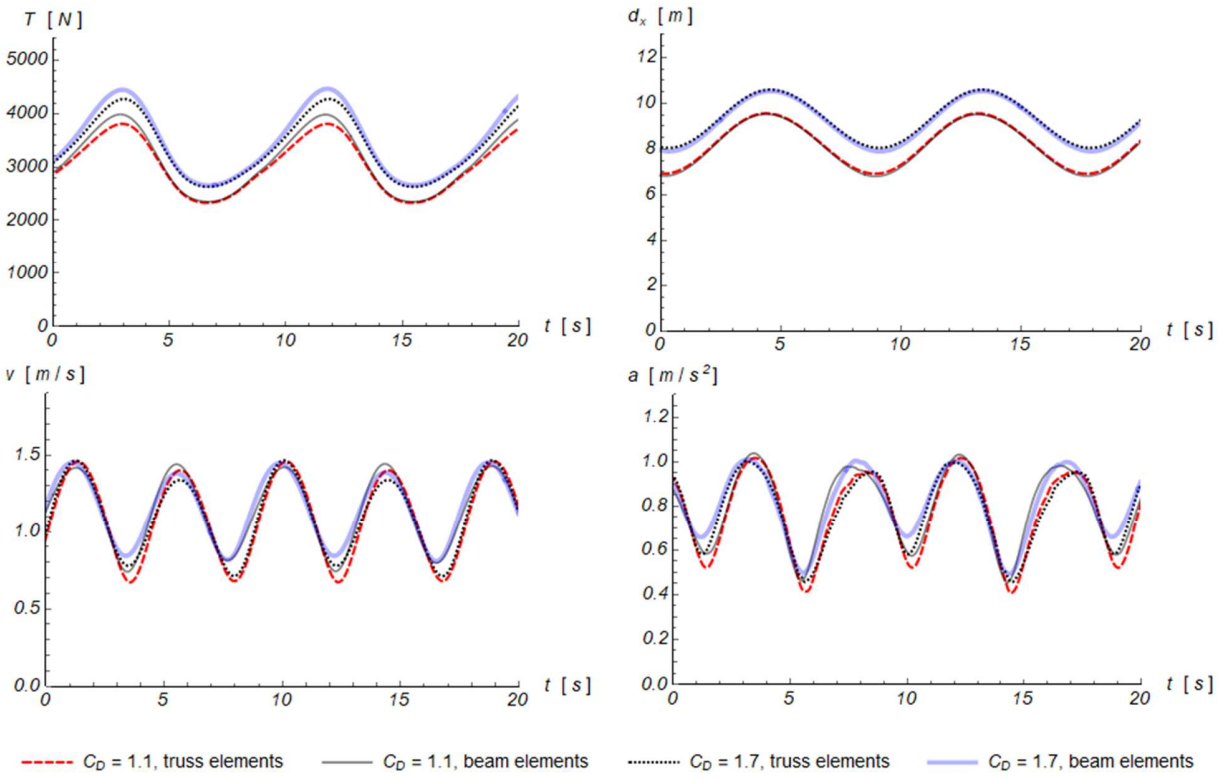

Figure 9. Drag coefficient and bending stiffness parametric study results in storm conditions. T is the mooring tension, and displacements d_x, velocities v and acceleration a are provided for the midpoint of the 4th dropper.

Table 8. Maximum values of tension, displacement, velocity and acceleration for truss and beam models with different dropper drag coefficients.

Drag coefficient, element type	$\boldsymbol{T}$ $[\boldsymbol{kN}]$	$\boldsymbol{d_x}$ $[\boldsymbol{m}]$	$\boldsymbol{v}$ $[\boldsymbol{m/s}]$	$\boldsymbol{a}$ $\left[\boldsymbol{m/s^2}\right]$
$\boldsymbol{C_D = 1.1}$**, truss elements**	3.80	9.57	1.45	1.01
$\boldsymbol{C_D = 1.1}$**, beam elements**	3.98	9.53	1.43	1.03
$\boldsymbol{C_D = 1.7}$**, truss elements**	4.27	10.60	1.46	1.00

$C_D = 1.7$, beam elements	4.46	10.54	1.45	0.99
Maximum deviation from $C_D = 1.3$, beam elements	7.6%	5.5%	1.3%	1.7%

5.3 Performance of mussel longline in fair and stormy weather

Four longline designs were considered, including the initial 2-anchor system (Fig. 6a), the modified 4-anchor system (Fig. 6b and b1), the 4-anchor system with around 10% of the dropper weight added to the lower end of each dropper (Fig. 6b and b2), and the 4-anchor system with three intermediate vertical anchor legs (Fig. 6c), as described in Sections 2.1 and 3.3. Each of these designs was numerically simulated in fair and storm environments with three different sleeve types, namely *yellow*, *blue* and *green* (Table 2). The collinear wave and current directions parallel to the seafloor and perpendicular to the mainline were chosen for these simulations since they had been found to cause an excessive structure motion in the original design. As output data, a maximum tension of the mooring line T at point *1* and maximum horizontal displacement d_x, velocity v, acceleration a, horizontal projection of relative velocity v_{rx}, vertical projection of relative velocity v_{rz} and vertical projection of acceleration a_z at points *2, 3, 4, 5* were chosen, see Fig. 10. All of the predicted results are summarized in Table A.1 and A.2, see Appendix.

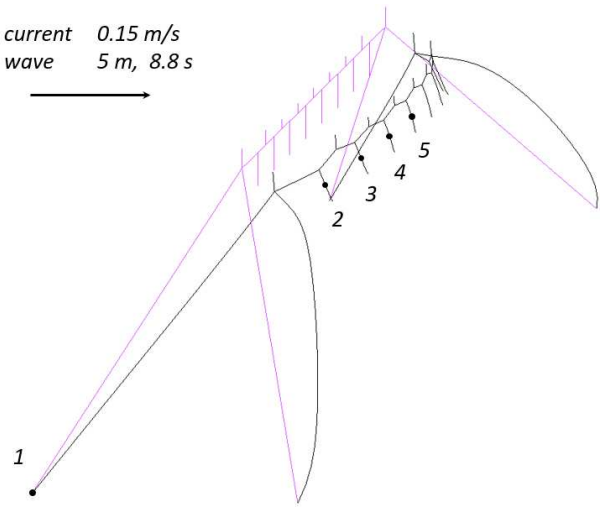

Figure 10. The 4-point mooring longline with *blue* droppers in storm conditions. Both current and wave are normal to the mainline. Tension is measured at mooring line attachment point *1*, while displacements, velocities and accelerations are monitored at points *2, 3, 4, 5*.

Fig. 11 presents results of the numerical simulations organized as a ratio of the maximum observed value of the mooring tension, horizontal displacement, dropper velocity, acceleration and vertical acceleration for a specific design to the corresponding value for basic 2-point mooring line configuration. Comparisons indicate that changing the basic 2-point mooring system (the present standard for field deployment) to the 4-point mooring system greatly reduces displacement (by 50-65%, depending on dropper type), but mooring tension, velocity and acceleration are usually the same or increase. Adding weight to the ends of the droppers, however, generally decreases mooring tension, velocity and acceleration with the vertical projection of acceleration reduced by 20-35%. Adding additional vertical legs with fixed anchoring decreases mooring tension and displacement by 20-30%, but velocity and acceleration are 1.66-1.79 times higher (Fig. 11). From the standpoint of mussel retention, only adding weight seems to have substantial beneficial effect. Extra model runs included the use of a circular heave plate attached to the bottom of each dropper to provide additional vertical drag and added mass, but numerical simulations did not show any advantage for such design. Also, the increase of a storm wave height from $5\,m$ to $9\,m$ resulted in increase of the motion response by about 30% for all considered configurations.

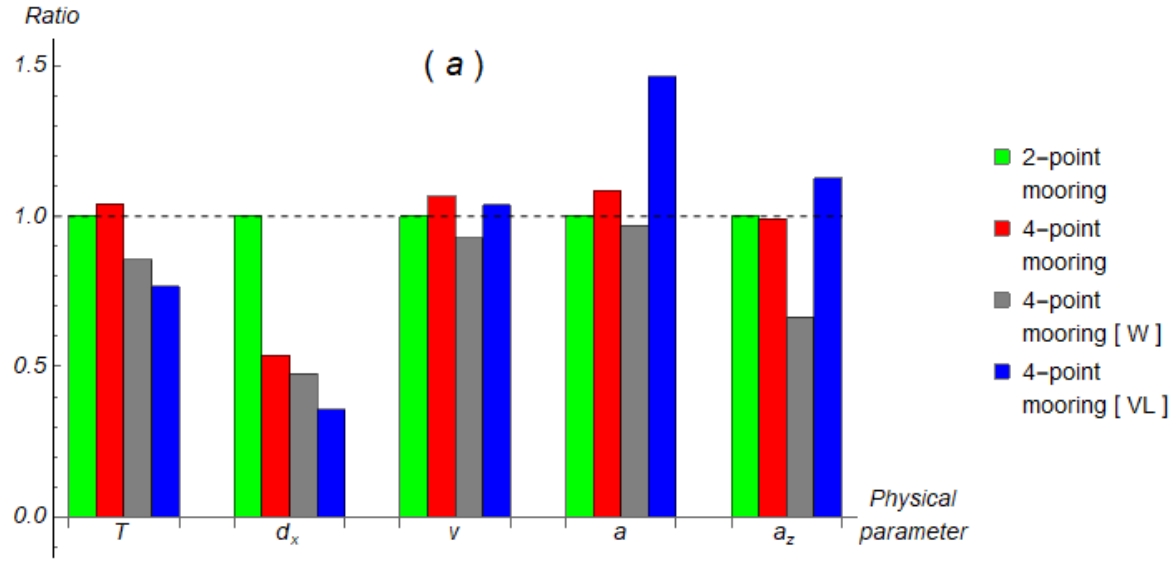

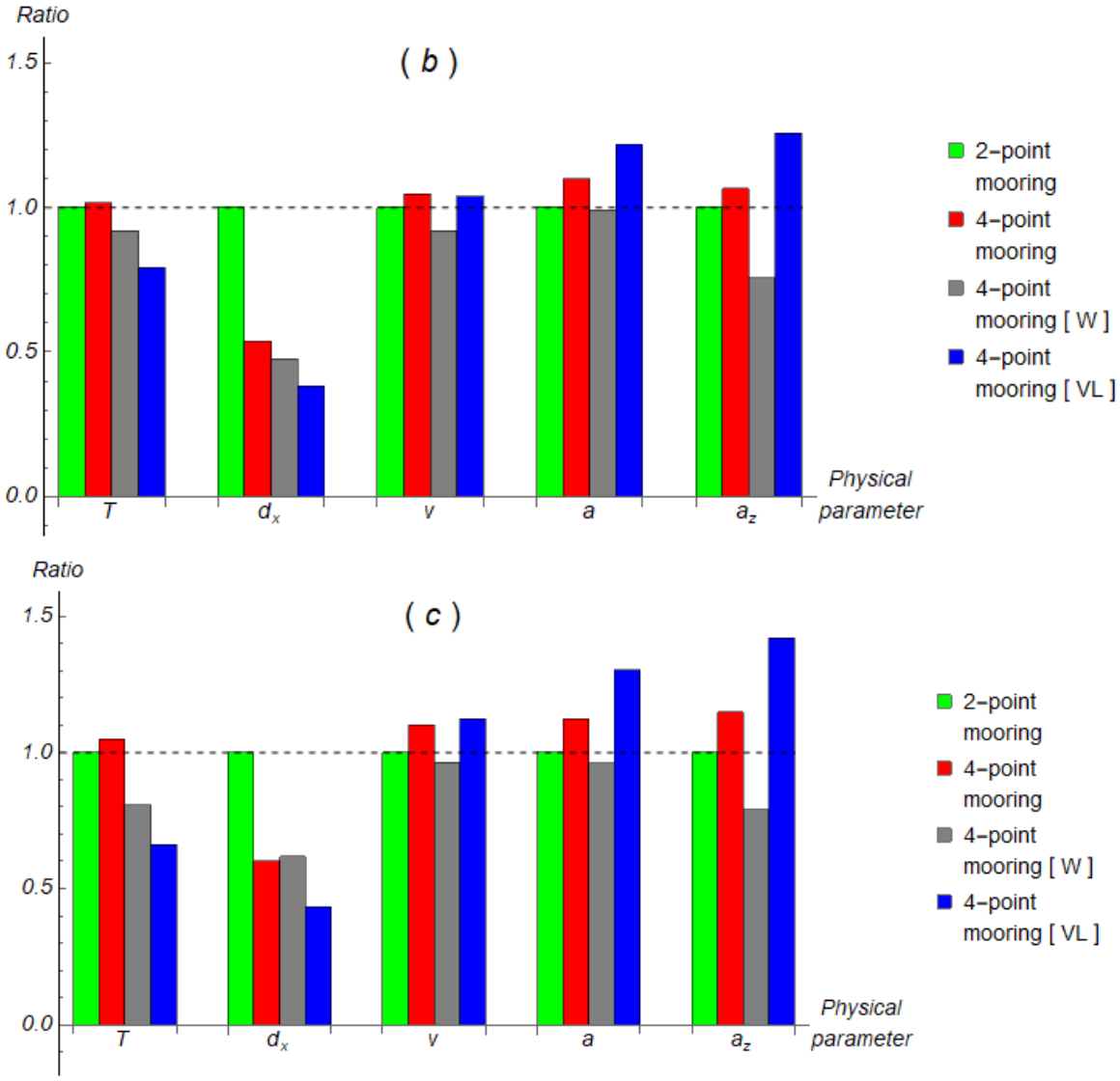

Figure 11. Ratio of the system response parameters to the corresponding values for the 2-point mooring design. Relative peak values of mooring tension T, horizontal displacement d_x, velocity v, acceleration a and its vertical projection a_z of four considered designs with *(a) yellow*, *(b) blue* and *(c) green* droppers. Mooring tension is the maximum predicted near the fixed anchors. Displacement, velocity and acceleration are maximum values predicted for droppers. The x-direction is in the direction of wave and current, and the z-direction

Fig. 12 provides results of the simulations as a ratio of the maximum predicted value of the system response parameters for a specific dropper type to the corresponding values for the weighted 4-point mooring line configuration with the *yellow* dropper. Comparison of different protective sleeve designs shows that their performance is directly correlated with the linear density and diameter, as determined by their mussel content. Utilization of the Vexar Superduty green sleeve resulted in much higher linear density of the dropper requiring more compensating floats and producing significantly

higher mooring line tensions and horizontal mainline displacements for both fair and stormy conditions, see Fig. 12. Note that in the case of fair weather, the absolute values of velocities and accelerations are very low, so small differences can lead to significant jumps in the ratios. For example, the absolute values of vertical acceleration for *blue* and *green* dropper are $0.02\,m/s^2$ and $0.01\,m/s^2$, and this small difference is shown as a 2 times reduction in Fig. 12a.

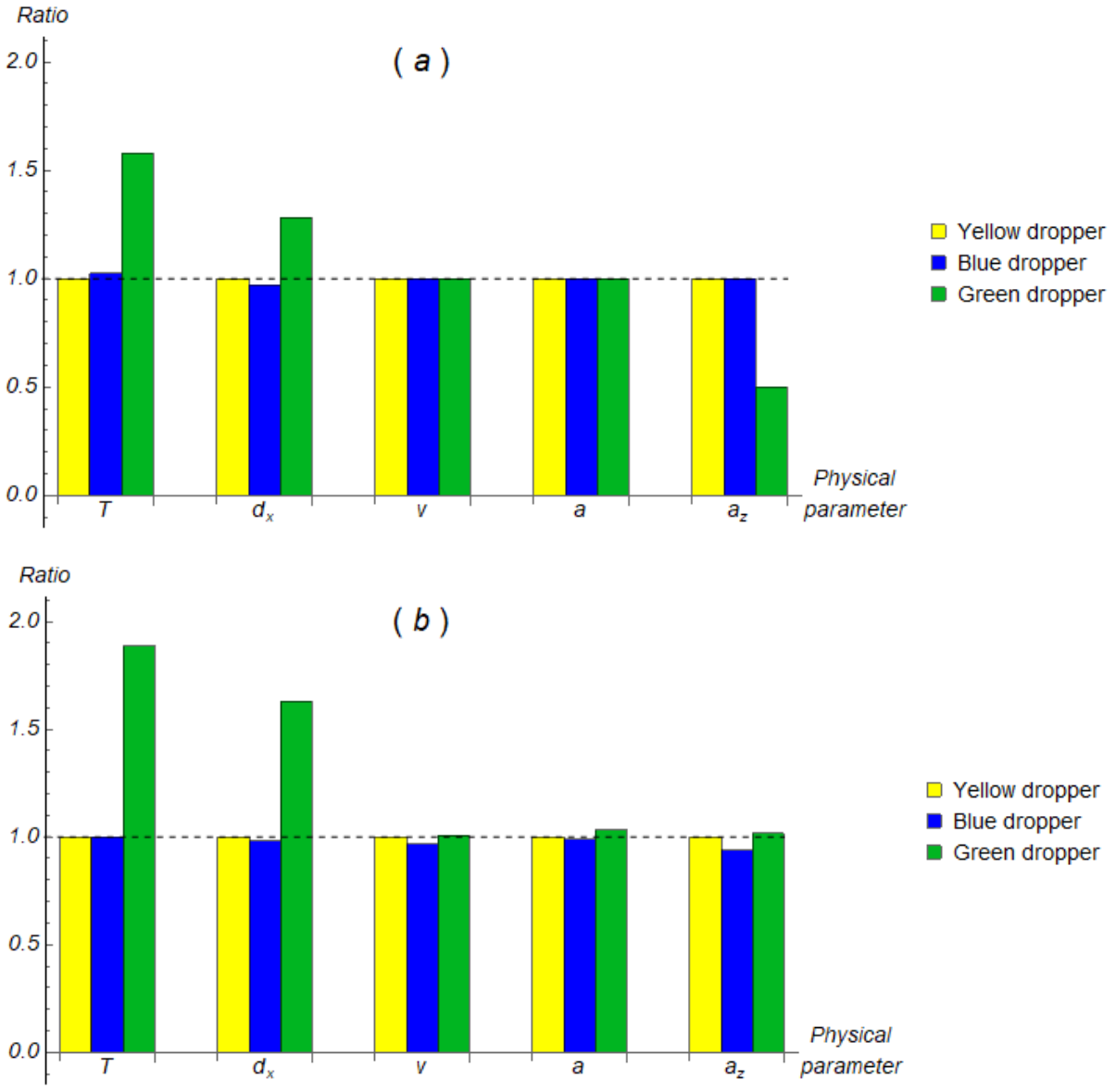

Figure 12. Ratio of the system response parameters to the corresponding values for the 4-point mooring [W] design with *yellow* dropper. Relative peak values of mooring tension T, horizontal displacement d_x, velocity v, acceleration a and its vertical projection a_z for four considered designs in *(a)* fair and *(b)* stormy weather. Mooring tension is the maximum predicted near the fixed anchors. Displacement,

velocity and acceleration are maximum values predicted for droppers. The x-direction is in the direction of wave and current, and the z-direction is upwards.

The simulation results presented in this section can be compared with other investigations of similar configurations. The offshore observations of a $189\ m$ long fully submerged mussel longline with 12 legs at $20-24\ m$ depth open ocean site (Gagnon and Bergeron, 2017) show that the ratio between the $0.6\ kN$ maximum tension and the $0.25\ kN$ pretension of mooring lines is around 2.4 (with maximum current velocity of $0.24\ m/s$, wave height of $3.5\ m$ and wave length of $96\ m$), while our 2-point mooring longline model with the *blue* droppers of the same diameter predicts a ratio of $3.65\ kN\ /\ 2.5\ kN = 1.46$ in storm conditions. However, for the rest of 4-point mooring models with $1.5\ kN$ pretension this ratio is somewhat higher, up to 2.47. Furthermore, their open ocean site observations report the maximum droppers' vertical acceleration $0.3\ m/s^2$, which is less than half the acceleration predicted in our numerical simulations for stormy weather. This discrepancy is caused by the difference in wave height, length and water depth, as well as design features, such as the number of additional legs, distribution of floats and droppers, etc. Nevertheless, a maximum inclination of 31° predicted by the numerical simulation in the present work is comparable to the maximum inclination of 24° from the observations.

Another offshore observation of a $150\ m$ long partially submerged mussel longline (Stevens et al., 2007) recorded maximum mooring line tensions from $6.0\ kN$ to $7.7\ kN$ and a maximum dropper acceleration of around $4.5\ m/s^2$ under a $0.16\ m/s$ tidal current in $11\ m$ water depth. It can be seen that their values are of a different order from ours, since the droppers are much closer to the water surface and, as a result, experience higher fluid velocities and accelerations.

At the same time, the numerical dynamic analysis of a $200\ m$ fully submerged mussel longline system presented in Raman-Nair et al., 2008 resulted in a wave-induced ($3\ m$ wave height, $8.5\ s$ wave period and $99.6\ m$ wave length) average mooring line tension of $1.25\ kN$ and a maximum tension of $2.25\ kN$. Although those tensions are of the same order as the ones presented in this paper, they are still around 35% lower due to an absence of the current, slightly different wave properties, different longline design and the wave propagation direction at 65.5° to the mainline.

6. Conclusions

Hydrodynamic modeling software *Hydro-FE* is demonstrated to be an efficient finite element numerical tool to predict structural response of flexible aquaculture installations subjected to offshore environmental loading conditions. It was used in the present study to evaluate the dynamic performance

of several simple submerged longline designs with different mussel droppers under the fair and stormy weather typical for the considered North Atlantic mussel farming site. The loading from waves was implemented using the linear Airy wave theory. The Reynolds number dependent drag coefficients were incorporated in the hydrodynamic forcing formulas. The equivalent dropper concept was proposed and verified to provide a good proxy model with statistically insignificant variations (under 5%) in all of the considered quantities of interest when compared to the predictions of the full model. This led to significant computational 3.5 times speed-up and improved performance of simulations.

Field measurements taken at the University of New Hampshire nearshore multi-trophic aquaculture site show that mechanical properties of mussel droppers are different for different sleeves and vary in diameter, mass and bending stiffness. Numerical simulations indicate that the effect of bending stiffness on the overall structural response of the considered mussel droppers is negligible. In addition, variations of the dropper normal drag coefficients in the reported range of values from 1.1 to 1.7 result in insignificant deviations (when compared to the margin of error of experimental measurements) from the predictions obtained for the commonly used value of 1.3: 7.6% in mooring tensions, 5.5% in the middle dropper displacements and 1.7% in its accelerations.

Combination of field measurements and numerical simulations has been used to evaluate the effect of various protective sleeves and structural designs on the performance of longline mussel farms. Comparisons show that adding 2 additional mooring lines to the basic 2-point mooring systems reduces horizontal displacement by 50-65%, depending on dropper type. Also, the weights attached to the ends of the droppers generally decrease their velocities and accelerations with the vertical projection of acceleration reduced by 20-35%. Additional vertical legs with fixed anchoring decrease mooring tensions and droppers' horizontal displacements by 20-30%, but velocities and accelerations are 1.66-1.79 times higher than in weighted configuration. From the standpoint of mussel retention, adding 2 mooring lines and weight seem to have some beneficial effects.

Although mussel farms are typically large operations with multiple longlines, this study was focused on modeling of the single mussel longline response for different environmental conditions. It is expected that the approach will be applicable to larger farms if modifications of environmental conditions, such as current shadowing and spatial variations in currents and waves are taken into account.

Overall, it has been demonstrated that the proposed model with the equivalent droppers provide a robust and computationally efficient engineering tool with strong predictive capability which was verified through the parametric studies and validated via the comparison to the existing field measurements. Thus, adoption of this tool by researchers and practitioners can enable model-based engineering flows for

designing optimal mussel farming systems with well-defined hydrodynamic response characteristics in the operational and storm conditions. We anticipate that this can yield improved accuracy in the predictions of the service life and reduced costs of the components required to build these systems.

Acknowledgements

This research was supported by Saltonstall Kennedy grant NA17NMF4270207 from National Oceanic and Atmospheric Administration. The authors would like to thank Peter Flanigan and Vincent Prien from Isles of Shoals Mariculture for the access to their mussels growing facility and data. We also express our gratitude to Arron Jones and Erich Berghahn from New Hampshire Sea Grant for their assistance with collecting data from the mussel farm.

References

Bansal, R.K., 2010. A textbook of strength of materials. Laxmi Publications.

Berstad, A.J., Heimstad, L.F., 2019. Analysis of Flexible Net Structures in Marine Environment. Marine 2019.

Berstad, A.J., Walaunet, J., Heimstad, L.F., 2012. Loads From Currents and Waves on Net Structures. https://doi.org/10.1115/omae2012-83757

Buck, B.H., 2007. Experimental trials on the feasibility of offshore seed production of the mussel Mytilus edulis in the German Bight: Installation, technical requirements and environmental conditions. Helgol. Mar. Res. 61, 87–101. https://doi.org/10.1007/s10152-006-0056-1

Buck, B.H., Langan, R., 2017. Aquaculture Perspective of Multi-Use Sites in the Open Ocean. https://doi.org/10.1007/978-3-319-51159-7

Cheney, D., Langan, R., Heasman, K., Friedman, B., Davis, J., 2010. Shellfish Culture in the Open Ocean: Lessons Learned for Offshore Expansion. Mar. Technol. Soc. J. 44, 55–67. https://doi.org/10.4031/MTSJ.44.3.6

Choo, Y.-I., Casarella, M.J., 1971. Hydrodynamic Resistance of Towed Cables. J. Hydronautics. https://doi.org/10.2514/3.62882

Cranford, P.J., Duarte, P., Robinson, S.M.C., Fernández-Reiriz, M.J., Labarta, U., 2014. Suspended particulate matter depletion and flow modification inside mussel (Mytilus galloprovincialis) culture rafts in the Ría de Betanzos, Spain. J. Exp. Mar. Bio. Ecol. https://doi.org/10.1016/j.jembe.2013.12.005

Danioux, C., Bompais, X., Paquotte, P., Loste, C., 2000. Offshore mollusc production in the

Mediterranean basin. Mediterr. offshore Maric. 140, 115–140.

Dean, R.G., Dalrymple, R.A., 1991. Water wave mechanics for engineers and scientists, Engineering.

DeCew, J., Tsukrov, I., Risso, A., Swift, M.R., Celikkol, B., 2010. Modeling of dynamic behavior of a single-point moored submersible fish cage under currents. Aquac. Eng. 43, 38–45. https://doi.org/10.1016/j.aquaeng.2010.05.002

Dewhurst, T., 2016. Dynamics of a Submersible Mussel Raft, PhD Thesis. Univ. New Hampsh.

Drapeau, A., Comeau, L.A., Landry, T., Stryhn, H., Davidson, J., 2006. Association between longline design and mussel productivity in Prince Edward Island, Canada. Aquaculture. https://doi.org/10.1016/j.aquaculture.2006.07.045

Fredriksson, D.W., Swift, M.R., Irish, J.D., Tsukrov, I., Celikkol, B., 2003. Fish cage and mooring system dynamics using physical and numerical models with field measurements. Aquac. Eng. https://doi.org/10.1016/S0144-8609(02)00043-2

Gagnon, M., Bergeron, P., 2017. Observations of the loading and motion of a submerged mussel longline at an open ocean site. Aquac. Eng. 78, 114–129. https://doi.org/10.1016/j.aquaeng.2017.05.004

Goodman, T., Breslin, J., 1976. Statics and dynamics of anchoring cables in waves. J. Hydronautics 10, 113–120.

Gosz, M., Kestler, K., Swift, M.R., Celikkol, B., 1996. Finite Element Modeling of Submerged Aquaculture Net-Pen Systems. Open Ocean Aquac. Proc. Int. Conf 8–10.

Hoerner, S., 1965. Fluid-Dynamic Drag. Publ. by author.

Karayücel, S., Çelik, M.Y., Karayücel, I., Öztürk, R., Eyüboğlu, B., 2015. Effects of stocking density on survival, growth and biochemical composition of cultured mussels (Mytilus galloprovincialis, Lamarck 1819) from an offshore submerged longline system. Aquac. Res. https://doi.org/10.1111/are.12291

Landmann, J., Ongsiek, T., Goseberg, N., Heasman, K., Buck, B., Paffenholz, J.-A., Hildebrandt, A., 2019. Physical Modelling of Blue Mussel Dropper Lines for the Development of Surrogates and Hydrodynamic Coefficients. J. Mar. Sci. Eng. https://doi.org/10.3390/jmse7030065

Langan, R., 2013. Mussel Culture, Open Ocean Innovations. Sustain. Food Prod. 1229–1239.

Lauzon-Guay, J.S., Barbeau, M.A., Watmough, J., Hamilton, D.J., 2006. Model for growth and survival of mussels Mytilus edulis reared in Prince Edward Island, Canada. Mar. Ecol. Prog. Ser. https://doi.org/10.3354/meps323171

Lee, C.W., Kim, Y.B., Lee, G.H., Choe, M.Y., Lee, M.K., Koo, K.Y., 2008. Dynamic simulation of a fish cage system subjected to currents and waves. Ocean Eng. https://doi.org/10.1016/j.oceaneng.2008.06.009

Lee, C.W., Lee, J., Park, S., 2015. Dynamic behavior and deformation analysis of the fish cage system using mass-spring model. China Ocean Eng. https://doi.org/10.1007/s13344-015-0022-2

Li, Y.C., Zhao, Y.P., Gui, F.K., Teng, B., 2006. Numerical simulation of the hydrodynamic behaviour of submerged plane nets in current. Ocean Eng. https://doi.org/10.1016/j.oceaneng.2005.11.013

Lin, J., Li, C., Zhang, S., 2016. Hydrodynamic effect of a large offshore mussel suspended aquaculture farm. Aquaculture. https://doi.org/10.1016/j.aquaculture.2015.08.039

López, J., Hurtado, C.F., Gómez, A., Zamora, V., Queirolo, D., Gutiérrez, A., Ciencias, E. De, Ciencias, F. De, Universidad, P., Valparaíso, C. De, 2017. Stress analysis of a submersible longline culture system through dynamic simulation. Lat. Am. J. Aquat. Res. 45, 25–32. https://doi.org/10.3856/vol45-issue1-fulltext-3

Morison, J.R., Johnson, J.W., Schaaf, S.A., 1950. The Force Exerted by Surface Waves on Piles. J. Pet. Technol. 2, 149–154. https://doi.org/10.2118/950149-G

Plew, D.R., 2005. The Hydrodynamic Effects of Long-line Mussel Farms. Univ. Canterbury 356 p.

Plew, D.R., Enright, M.P., Nokes, R.I., Dumas, J.K., 2009. Effect of mussel bio-pumping on the drag on and flow around a mussel crop rope. Aquac. Eng. 40, 55–61. https://doi.org/10.1016/j.aquaeng.2008.12.003

Plew, D.R., Stevens, C.L., Spigel, R.H., Hartstein, N.D., 2005. Hydrodynamic implications of large offshore mussel farms. IEEE J. Ocean. Eng. 30, 95–108. https://doi.org/10.1109/JOE.2004.841387

Raman-Nair, W., Colbourne, B., 2003. Dynamics of a mussel longline system. Aquac. Eng. 27, 191–212. https://doi.org/10.1016/S0144-8609(02)00083-3

Raman-Nair, W., Colbourne, B., Gagnon, M., Bergeron, P., 2008. Numerical model of a mussel longline system: Coupled dynamics. Ocean Eng. 35, 1372–1380. https://doi.org/10.1016/j.oceaneng.2008.05.008

Reite, K.-J., Føre, M., Aarsæther, K.G., Jensen, J., Rundtop, P., Kyllingstad, L.T., Endresen, P.C., Kristiansen, D., Johansen, V., Fredheim, A., 2014. FHSIM — Time Domain Simulation of Marine Systems. https://doi.org/10.1115/omae2014-23165

Stevens, C., Plew, D., Hartstein, N., Fredriksson, D., 2008. The physics of open-water shellfish aquaculture. Aquac. Eng. 38, 145–160. https://doi.org/10.1016/j.aquaeng.2008.01.006

Stevens, C.L., Plew, D.R., Smith, M.J., Fredriksson, D.W., 2007. Hydrodynamic Forcing of Long-Line Mussel Farms: Observations. J. Waterw. Port, Coastal, Ocean Eng. https://doi.org/10.1061/(asce)0733-950x(2007)133:3(192)

Tsarau, A., Kristiansen, D., 2019. Application of FhSim for the Analysis of Environmental Loads on a Complete Fish-Farm System. Marine 2019.

Tsukrov, I., Eroshkin, O., Fredriksson, D., Swift, M.R., Celikkol, B., 2002. Finite element modeling of net panels using a consistent net element. Ocean Eng. 30, 251–270. https://doi.org/10.1016/S0029-8018(02)00021-5

Tsukrov, I.I., Ozbay, M., Swift, M.R., Celikkol, B., Fredriksson, D.W., Baldwin, K., 2000. Open Ocean Aquaculture Engineering: Numerical Modeling. Mar. Technol. Soc. J. 34, 29–40. https://doi.org/10.4031/MTSJ.34.1.4

Zhao, Y., Yang, H., Bi, C., Chen, Q., Dong, G., Cui, Y., 2019. Hydrodynamic responses of longline aquaculture facility with lantern nets in waves. Aquac. Eng. 86, 101996. https://doi.org/10.1016/j.aquaeng.2019.101996

Zhao, Y.P., Li, Y.C., Dong, G.H., Gui, F.K., Teng, B., 2007. A numerical study on dynamic properties of the gravity cage in combined wave-current flow. Ocean Eng. https://doi.org/10.1016/j.oceaneng.2007.05.003

Zhao, Y.P., Wang, X.X., Decew, J., Tsukrov, I., Bai, X.D., Bi, C.W., 2015. Comparative study of two approaches to model the offshore fish cages. China Ocean Eng. 29, 459–472.

https://doi.org/10.1007/s13344-015-0032-0

Appendix. Maximum values of tensions, displacements, velocities and accelerations predicted for various dropper types, mooring designs and environmental loading conditions.

Table A.1. Fair weather maximum values of mooring tension T, horizontal displacement d_x, velocity v, projections of relative velocity v_{rx}, v_{rz}, acceleration a and its vertical projection a_z. Mooring tension is the maximum predicted near the fixed anchors. Displacement, velocity and acceleration are maximum values predicted for droppers. The x-direction is in the direction of wave and current, and the z-direction is upwards.

Yellow dropper	$T\ [kN]$	$d_x\ [m]$	$v\ [m/s]$	$v_{rx}\ [m/s]$	$v_{rz}\ [m/s]$	$a\ [m/s^2]$	$a_z\ [m/s^2]$
2-point mooring	2.49	7.16	0.07	0.17	0.06	0.11	0.05
4-point mooring	1.85	2.73	0.07	0.18	0.04	0.12	0.03
4-point mooring [W]	2.09	2.48	0.06	0.17	0.02	0.10	0.02
4-point mooring [VL]	1.62	1.95	0.07	0.19	0.04	0.13	0.07

Blue dropper	$T\ [kN]$	$d_x\ [m]$	$v\ [m/s]$	$v_{rx}\ [m/s]$	$v_{rz}\ [m/s]$	$a\ [m/s^2]$	$a_z\ [m/s^2]$
2-point mooring	2.57	6.95	0.06	0.17	0.02	0.10	0.04
4-point mooring	1.89	2.65	0.07	0.17	0.04	0.12	0.03
4-point mooring [W]	2.14	2.41	0.06	0.17	0.02	0.10	0.02
4-point mooring [VL]	1.60	2.18	0.06	0.18	0.01	0.10	0.06

Green dropper	$T\ [kN]$	$d_x\ [m]$	$v\ [m/s]$	$v_{rx}\ [m/s]$	$v_{rz}\ [m/s]$	$a\ [m/s^2]$	$a_z\ [m/s^2]$
2-point mooring	3.95	8.42	0.05	0.17	0.04	0.08	0.02
4-point mooring	3.08	3.38	0.05	0.17	0.03	0.09	0.01
4-point mooring [W]	3.30	3.18	0.06	0.18	0.02	0.10	0.01
4-point mooring [VL]	2.77	2.61	0.08	0.17	0.06	0.12	0.05

Table A.2. Storm conditions maximum values of mooring tension T, horizontal displacement d_x, velocity v, projections of relative velocity v_{rx}, v_{rz}, acceleration a and its vertical projection a_z. Mooring tension is the maximum predicted near the fixed anchors. Displacement, velocity and acceleration are maximum values predicted for droppers. The x-direction is in the direction of wave and current, and the z-direction is upwards.

Yellow dropper	$T\ [kN]$	$d_x\ [m]$	$v\ [m/s]$	$v_{rx}\ [m/s]$	$v_{rz}\ [m/s]$	$a\ [m/s^2]$	$a_z\ [m/s^2]$
2-point mooring	3.92	18.16	1.36	0.40	0.46	0.95	0.95
4-point mooring	4.08	9.75	1.45	0.49	0.42	1.03	0.94
4-point mooring [W]	3.35	8.67	1.26	0.42	0.57	0.92	0.63
4-point mooring [VL]	3.00	6.51	1.41	0.51	0.82	1.39	1.07

Blue dropper	$T\ [kN]$	$d_x\ [m]$	$v\ [m/s]$	$v_{rx}\ [m/s]$	$v_{rz}\ [m/s]$	$a\ [m/s^2]$	$a_z\ [m/s^2]$
2-point mooring	3.65	17.87	1.33	0.37	0.73	0.92	0.78
4-point mooring	3.71	9.60	1.39	0.44	0.50	1.01	0.83
4-point mooring [W]	3.35	8.50	1.22	0.39	0.61	0.91	0.59
4-point mooring [VL]	2.89	6.83	1.38	0.47	0.83	1.12	0.98

Green dropper	$T\ [kN]$	$d_x\ [m]$	$v\ [m/s]$	$v_{rx}\ [m/s]$	$v_{rz}\ [m/s]$	$a\ [m/s^2]$	$a_z\ [m/s^2]$
2-point mooring	7.84	22.87	1.32	0.52	0.29	0.99	0.81
4-point mooring	8.23	13.75	1.45	0.56	0.26	1.11	0.93
4-point mooring [W]	6.32	14.12	1.27	0.56	0.44	0.95	0.64
4-point mooring [VL]	5.18	9.91	1.48	0.66	0.89	1.29	1.15